

Coexistence of Robust Edge States and Superconductivity in Few-Layer Stanene

Chenxiao Zhao,¹ Leiqiang Li,² Liying Zhang^{3,4}, Jin Qin,¹ Hongyuan Chen,¹ Bing Xia,¹ Bo Yang,¹ Hao Zheng,^{1,5,6} Shiyong Wang,^{1,5,6} Canhua Liu,^{1,5,6} Yaoyi Li,^{1,5,6} Dandan Guan,¹ Ping Cui^{2,*}, Zhenyu Zhang², and Jinfeng Jia^{1,5,6,†}

¹Key Laboratory of Artificial Structures and Quantum Control (Ministry of Education), Shenyang National Laboratory for Materials Science, School of Physics and Astronomy, Shanghai Jiao Tong University, Shanghai 200240, China

²International Center for Quantum Design of Functional Materials (ICQD), Hefei National Laboratory for Physical Sciences at Microscale (HFNL), and CAS Center for Excellence in Quantum Information and Quantum Physics, University of Science and Technology of China, Hefei, Anhui 230026, China

³Key Laboratory for Special Functional Materials of Ministry of Education, Collaborative Innovation Center of Nano Functional Materials and Applications, School of Materials Science and Engineering, Henan University, Kaifeng 475004, China

⁴International Laboratory for Quantum Functional Materials of Henan and School of Physics and Microelectronics, Zhengzhou University, Zhengzhou 450001, China

⁵Tsung-Dao Lee Institute, Shanghai Jiao Tong University, Shanghai 200240, China

⁶CAS Center for Excellence in Topological Quantum Computation, University of Chinese Academy of Sciences, Beijing 100190, China

 (Received 10 October 2021; accepted 31 March 2022; published 17 May 2022)

High-quality stanene films have been actively pursued for realizing not only quantum spin Hall edge states without backscattering, but also intrinsic superconductivity, two central ingredients that may further endow the systems to host topological superconductivity. Yet to date, convincing evidence of topological edge states in stanene remains to be seen, let alone the coexistence of these two ingredients, owing to the bottleneck of growing high-quality stanene films. Here we fabricate one- to five-layer stanene films on the Bi(111) substrate and observe the robust edge states using scanning tunneling microscopy/spectroscopy. We also measure distinct superconducting gaps on different-layered stanene films. Our first-principles calculations further show that hydrogen passivation plays a decisive role as a surfactant in improving the quality of the stanene films, while the Bi substrate endows the films with nontrivial topology. The coexistence of nontrivial topology and intrinsic superconductivity renders the system a promising candidate to become the simplest topological superconductor based on a single-element system.

DOI: [10.1103/PhysRevLett.128.206802](https://doi.org/10.1103/PhysRevLett.128.206802)

Synergy between nontrivial topology and superconductivity is appealing for the potential realization of topological superconductors (TSCs) [1–3], which may further harbor Majorana zero modes critically needed for topological quantum computing [4]. The prevailing approach towards this goal is to induce superconductivity in materials with strong spin-orbit coupling via proximity effect—i.e., creating heterostructures combining topological insulators or nanowire or atom chains and traditional superconductors [5–10]. In this endeavor, standing challenges include precise control of the interfacial structures and limited decay length of the proximity effect. An alternative pathway is to supersede the external proximity between different materials' components by an internal type (termed the self-proximity effect), referring to bridging between the bulk states and nontrivial boundary states within a single material. Compelling examples include the recently discovered Fe(Te,Se) [11–13], Li(Fe,Co)As [14], and (Li,Fe)OHFeSe systems [15]. Here the dominant challenge lies in the unavoidable stoichiometric inhomogeneities in such multicomponent three-dimensional (3D) crystals. To date, 2D candidate systems possessing such self-proximity effects are still lacking; nevertheless, the newly

reported intrinsic superconductivity in few-layer stanene [16,17], which is also a candidate for a 2D quantum spin Hall insulator (QSHI) [18], serves as new animation for the exploration of stanene as a topological superconductor.

Stanene has been actively pursued since it was proposed to be a 2D QSHI [18]. Its simple structure and large inverted band gap make it an outstanding candidate to realize a QSHI [18]. Theoretical studies have shown that stanene films possess tunable topological properties that are sensitive to the substrate, chemical functionalization, and layer thickness [18–23]. Such sensitivities, in turn, pose challenges in the experimental realization of the nontrivial phase. As a result, a clear and robust evidence of the 1D topological edge states as characterized by the well-localized distribution of the density of states (DOS) at the island and film edges remains to be seen. In previous studies, monolayered stanene films with compressed strain were shown to exhibit only a trivial band structure [24–27]. An advance in realizing nontrivial band topology was achieved when growing stanene on the Cu(111)-(2 × 2) surface, where an inverted band order was observed in the ultraflat yet metastable stanene films [28]. Indications of edge states of monolayered stanene grown on

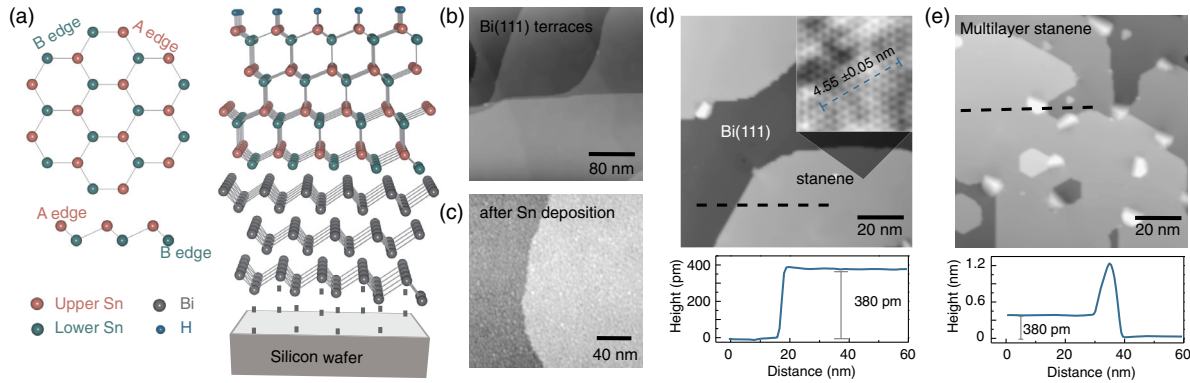


FIG. 1. (a) Schematics of a freestanding monolayer stanene (left) and a sample structure of four-layer stanene/Bi(111)/Si with the top surface of stanene passivated by hydrogen (right). (b),(c) Topographies of the Bi(111) substrate before [(b): $V_s = 2.00$ V, $I_{\text{set}} = 100$ pA] and after [(c): $V_s = 2.27$ V, $I_{\text{set}} = 50$ pA] depositing Sn. (d) Topography of the first-layer stanene films on Bi(111) after annealing, with a profile shown at the bottom depicting the height along the black dotted line. $V_s = 2.0$ V, $I_{\text{set}} = 70$ pA. Inset: atomically resolved image taken on the stanene film. (e) Topography of multilayer stanene (~ 2.5 layers) on Bi(111), with the corresponding height profile shown below. $V_s = 2.7$ V, $I_{\text{set}} = 80$ pA.

the InSb(111)-(3×3) substrate have also been reported, even though the films contain pronounced defects [29]. At a separate front, superconductivity has been observed in few-layer stanene grown on PbTe(111) [16,17], albeit verified to be topologically trivial [27]. Therefore, identification of a proper substrate to grow stable stanene films with nontrivial topological properties and intrinsic superconductivity is critically needed for further exploration and potential utilization of their salient properties and functionalities.

In this Letter, we devise a novel kinetic pathway to grow successfully one- to five-layered stanene with high quality on the Bi(111) substrate, where the stanene films are stable at room temperature and exhibit the long-sought edge states and superconducting properties. Our *in situ* scanning tunneling microscopy and spectroscopy (STM and STS) measurements confirm the quality of the stanene films as well as the robust edge states in all the one- to five-layered films. Furthermore, distinct superconducting gaps on different-layered stanene films are detected. Our first-principles calculations reveal that hydrogen passivation plays a decisive role as a surfactant in facilitating the multilayer growth and improving the overall quality of the stanene films, while the Bi(111) substrate endows the films with nontrivial topology irrespective of the layer thickness. The present findings open an appealing avenue toward platforms that combine nontrivial topology and superconductivity, the two central ingredients of topological superconductivity, all based on a simple single-element system.

The Bi(111) film is chosen as the substrate to grow stanene based on our recent prediction of achieving high-quality stanene film on a Bi precovered Bi_2Te_3 surface [30]. As illustrated in Fig. 1(a), the Bi(111) films were first grown on a silicon wafer with the film thickness of ~ 10 nm to eliminate the epitaxial strain with silicon. The epitaxial growth of stanene was carried out at low temperature to get

evenly covered Sn atoms on the Bi(111) surface [Fig. 1(c)], followed by annealing at 40°C , after which the Sn atoms form stanene films with good quality, as shown in Fig. 1(d). The profile along the black dotted line in Fig. 1(d) indicates the height of a single stanene layer of ~ 0.38 nm. The atomically resolved image consisting of the upper-sublattice Sn atoms shows a hexagonal structure with a lattice constant of ~ 0.455 nm, which is the same as that of the Bi(111) substrate. Multilayered stanene films have also been achieved, with a slightly increased number of Sn clusters of $1 \sim 2$ nm in height residing at the film edges [Fig. 1(e)]. Specifically, we have obtained one- to five-layered stanene films. It should be emphasized that the topmost surface of the stanene films is saturated by hydrogen atoms based on previous experiences [24,27]. Our current experimental results and systematic first-principles calculations further reveal that the surface passivation of the growth front by the residual hydrogen is essential in achieving layer-by-layer growth of the high-quality stanene films, with the hydrogen functioning as a surfactant [31,32]. Details of the growth mechanism are presented in the Supplemental Material [33].

The existence of an energy gap separating occupied and unoccupied states is essential for QSHIs [55]. Our first-principles calculations show that the one- to five-layered stanene films on Bi(111) all have well-defined continuous gaps across the whole Brillouin zone with the inclusion of the spin-orbit coupling (SOC) (see Sec. VI of the Supplemental Material [33]). The topological invariant Z_2 is further evaluated as shown in the last row of Table I, indicating an extraordinarily robust nontrivial value that is impervious to the layer thickness.

Taking the four-layer stanene as an example, the conduction and valence bands are separated by a continuous gap exceeding 200 meV [Fig. 2(a)], and the indirect overlap between them characterizes the system to be a semimetal. The experimentally detected dI/dV spectrum in the interior

TABLE I. Z_2 invariants of different-layered stanene films under different conditions.

Conditions	Thickness					
	Z_2	1-layer	2-layer	3-layer	4-layer	5-layer
w/o Bi	w/o H	1	0	1	0	1
w/o Bi	w/H	0	0	1	1	1
w/Bi	w/o H	1	1	1	1	1
w/Bi	w/H					
(experimental condition)		1	1	1	1	1

of the fourth-layer stanene film (hereafter referred to as the bulk spectrum) is compared with the calculated DOS in Fig. 2(b). Here an upward shift of the Fermi level is applied for the calculated DOS because the three-bilayer Bi(111) substrate in the calculational model contributes to a lower electron doping level, compared with the much thicker experimental substrate (~ 10 nm). In doing so, the calculated DOS matches well with the dI/dV spectrum, especially within the energy window of -0.2 to 0.5 eV, overlapping the continuous gap. A remarkable feature in this range is the

observed bulk dip above the Fermi level, showing the lowest density of the bulk states and thereby giving a favorable window to better detect the edge states. Typical bulk spectra taken on stanene films with different layer thicknesses are compared in Fig. S7 in the Supplemental Material, all of which exhibit similar dip features [33].

The hallmark of the QSH systems are the topologically protected helical edge states, which are manifested by the enhanced intensity of local DOS (LDOS) at the film edges in spatially resolved STM studies [56–60]. Figure 2(c) shows a fourth-layer stanene island with a hexagonal shape sitting on a three-layer stanene film, which contains two different zigzag edges [the A and B edges, also shown in Fig. 1(a), with details to experimentally distinguish them given in Fig. S4 in the Supplemental Material [33]]. We compare the dI/dV spectra taken in the bulk and at the two edges in Fig. 2(d). The bulk spectrum shows the characteristic dip feature between 160 and 322 mV as marked by the vertical gray dashed lines, and the bulk dip minimum is located at ~ 185 mV. At both edges, the intensities of the LDOS surpass that of the bulk spectrum essentially in the whole dip range. The enhanced LDOS at both edges signifies the potential existence of the edge states. To visualize the energy

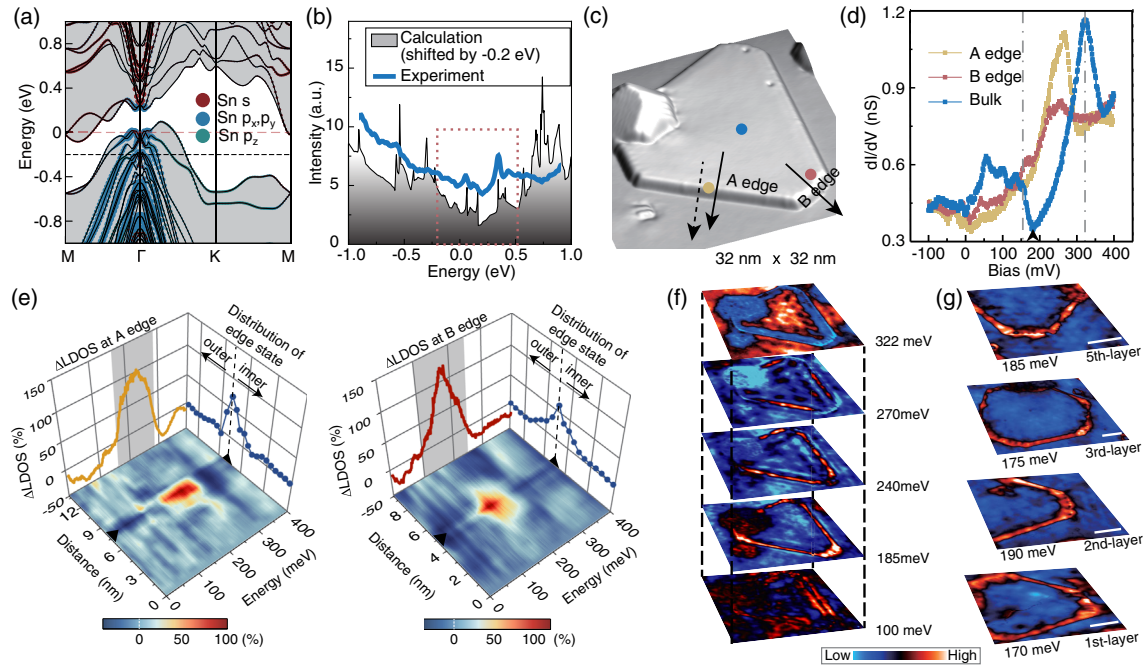


FIG. 2. (a) Calculated band structure (shifted) of a four-layer stanene film on Bi(111) with contributions from different Sn orbitals highlighted. (b) Comparison between calculated DOS and experimentally detected dI/dV spectrum of the four-layer stanene film on Bi(111). The dotted lines highlight the well-matched low-energy range around the Fermi level. (c) Topography of a fourth-layer stanene island with a hexagonal shape. $V_s = 2.0$ V, $I_{\text{set}} = 80$ pA. (d) dI/dV spectra taken in the interior and at the A or B edge of the island shown in (c). $I_{\text{set}} = 250$ pA, $V_{\text{mod}} = 3$ mV (961 Hz). (e) 3D plots of the Δ LDOSs as a function of energy and spatial distance along the black arrows in (c) crossing the A (left) and B (right) edges. The Δ LDOSs at the respective edges with positions marked by the black triangles are projected on the sidewalls, with the gray shadowed areas showing the energy windows dominated by the edge states (Δ LDOS > 0). The spatial variations of the edge states are projected by the blue curves. (f) dI/dV mappings of the stanene island shown in (c) at different energies. (g) dI/dV mappings of different-layered stanene islands taken at the energy of the respective bulk dip minimum. White scale bars: 5 nm. $I_{\text{set}} = 250$ pA, $V_{\text{mod}} = 3$ mV (961 Hz) for (f) and (g). dI/dV spectra were taken at 4.2 K.

distribution and spatial variation of the edge states, the spatially resolved relative differences of the LDOS [denoted by ΔLDOS s and defined as $(\text{LDOS}-\text{LDOS}_{\text{bulk}})/\text{LDOS}_{\text{bulk}}$] across the A or B edges [along the solid black arrows in Fig. 2(c)] are shown in Fig. 2(e), with detailed processes depicted in Fig. S11 in the Supplemental Material [33]. Clear evidence of the edge states can be observed as manifested by the localized red areas at both edges, but within slightly different energy windows. The ΔLDOS s at both edge positions are projected on the sidewalls by the yellow and red curves, highlighting the dominance of the edge states within the energy windows of 165–285 meV and 100–245 meV at the A and B edges, respectively. To further display the spatial distributions of the electronic states within both windows over the whole island, a series of dI/dV mappings ranging from 100 to 322 meV have been taken [Fig. 2(f)]. According to the mappings, the LDOS at about 185 meV, corresponding to the bulk dip minimum, is well localized and highly pronounced at both edges, which can be accounted for by the localized distribution of the edge states. We also note that the lacking of interference patterns in the interior of the island indicates the 1D character of the dominant electronic states at this energy.

We have further studied the penetration depths of the robust edge states by integrating the spatially resolved ΔLDOS s over the respective energy windows for the A and B edges (see details in Fig. S11 in the Supplemental Material [33]). The results are displayed on the sidewalls by the blue curves in Fig. 2(e), showing that the edge states have bilateral penetration depths (including inner and outer sides) of less than 4 nm for the A edge and 5 nm for the B edge. The rather short outward penetration depth at the A edge is understandable, since it is terminated by the Sn atoms in the upper sublattice, which have much weaker coupling with the lower-layer stanene. In contrast, the B edge is composed of the Sn atoms in the lower sublattice, which are strongly coupled with the lower-layer stanene, resulting in nearly symmetric penetration depths outwards and inwards.

Based on the results presented above, we infer that the robust edge states exist at both the A and B edges, especially highlighting themselves around the bulk dip minimum. These experimental findings are also valid for stanene films with different layer thicknesses. Figure 2(g) shows the dI/dV mappings of the stanene films of one to three and five layers, taken at the respective bulk dip minimum, where universal enhancements of the LDOS highlight the edge contours (see Fig. S12 in the Supplemental Material for the corresponding dI/dV spectra [33]). Furthermore, possible origins for topologically trivial edge states such as dangling bonds or H-passivation at the edges are also discussed and excluded by a comparative experiment of growing stanene on Bi_2Te_3 [33].

So far, our STM studies and first-principles calculations indicate that all the one- to five-layered stanene films on

Bi(111) are promising candidates of QSH systems. This observation is quite striking, because in typical situations, the stacking of QSHI layers would alter the topological invariant and result in an odd-even oscillation of the Z_2 [61]. This layer dependence of the topology is absent in our systems, at least up to five layers. This is shown in Table I, where we compare the Z_2 number of different-layer stanene under different conditions: with/without Bi substrate, and with/without H-passivation. The physical origin of the robust nontrivial Z_2 invariants is the consequence of interfacial coupling with the Bi(111) substrate (see detailed analyses in Sec. VI of the Supplemental Material [33]). Qualitatively, the Bi(111) substrate, with inherently strong SOC, is able to promote the nontrivial topology in the few-layer stanene via effective proximity effects [62,63].

Next, we investigate the superconducting properties of the stanene films at 400 mK. As shown in Fig. 3(a), clear superconducting gaps [taken along the dotted arrow in Fig. 2(c)] are detected on the same island where we have witnessed the robust edge states. The coherence peaks of these superconducting gaps exhibit spatial modulations owing to the scattering of electronic states near the edge. Figure 3(b) further shows the layer-dependent superconductivity of the stanene films, exhibiting a wider and deeper superconducting gap with a thicker layer. We note that the spectra which are taken on a fully complete stanene film of thickness n show noticeable difference from that taken on an island of the same height n [the latter labeled as a $(n-0.5)$]. In distinct contrast with earlier reports [16], here the existence of a superconducting gap is also observed for monolayer stanene, which might be enabled by the higher charge transfer level from the Bi(111) substrate. Full gaps against thermal excitations at 400 mK are obtained when the thickness reaches 3.5 layers or higher. The gaps (Δ) extracted by half the energy distance of two coherence peaks are plotted in Fig. 3(c), together with the zero bias conductance (ZBC) that quantizes the degree of the superconducting gap compared with a full gap. It can be seen that Δ increases rapidly with the thickness, saturating at ~ 1.5 layers; in contrast, ZBC decreases much more slowly, saturating until ~ 3.5 layers.

To further confirm that the observed gaps originate from superconducting pairing rather than other orders, we apply an external magnetic field to examine the attenuation of the pairing intensity. Figure 3(d) shows the evolution of the superconducting gap with an increasing out-of-plane magnetic field, taken on a 2.5-layer stanene film. The upper critical field (H_{c2}^{\perp}) was estimated to be larger than 0.4 T, which is larger than that for stanene on PbTe(111) [17]. This additional enhancement in H_{c2}^{\perp} may be related to the proximity-enhanced SOC by interfacing with Bi(111) (see more discussion in Sec. X of the Supplemental Material [33]).

Differently from previous 2D material platforms towards TSCs which otherwise require the participation of the

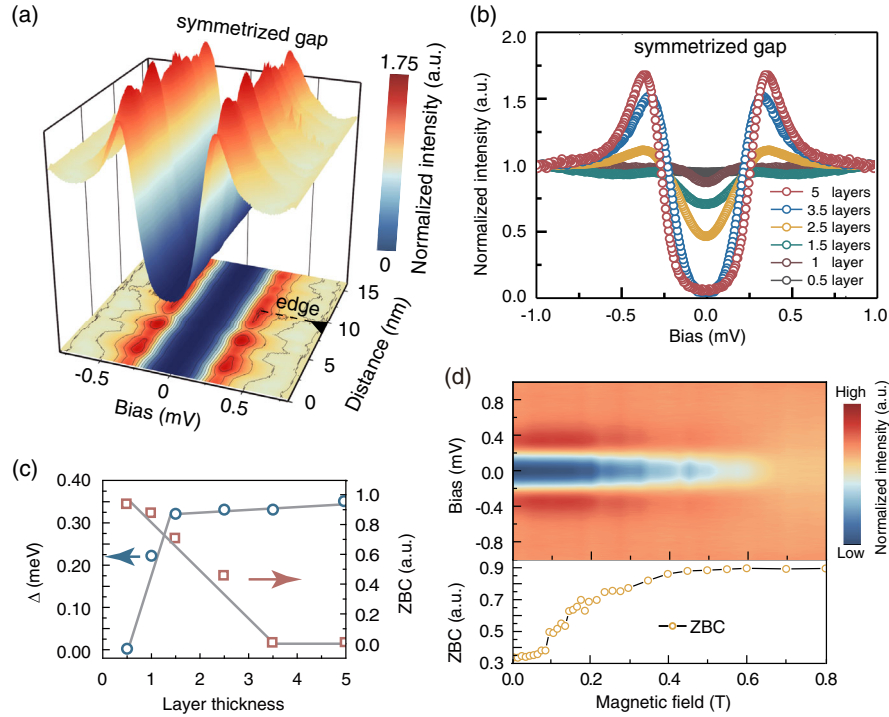


FIG. 3. (a) Spatial variation of the superconducting gap crossing the A edge along the dotted arrow in Fig. 2(c). The contour map is projected underneath. $I_{\text{set}} = 250$ pA, $V_{\text{mod}} = 20$ μ V (961 Hz). (b) Layer-dependent superconducting gap of stanene films. $I_{\text{set}} = 250$ pA, $V_{\text{mod}} = 20$ μ V (961 Hz). (c) Variations of the superconducting gap (Δ) and the ZBC with the layer thickness. (d) Attenuation of superconductivity under an out-of-plane magnetic field, taken on a third-layer stanene island. All the superconducting gaps in this figure are symmetrized and normalized by the intensity of the normal states at the starting bias.

proximity effects associated with an additional s -wave superconductor [10,64–66], or additional electrical gates [67,68], here both the ingredients of nontrivial topology and superconductivity are inherently present in few-layer stanene. In particular, an inherent self-proximity effect exists between the bulk and topological edge states of stanene as long as the edge states cross the Fermi level, resulting in the 1D TSC (see more discussion in Sec. X of the Supplemental Material [33]).

In conclusion, we have experimentally fabricated one- to five-layered high-quality stanene films on Bi(111), which have been shown to exhibit the robust 1D edge states and superconductivity. Our first-principles calculations have further revealed that hydrogen passivation plays a decisive role as a surfactant in improving the quality of stanene films, while the Bi substrate endows the films with nontrivial topology. The interplay between strong SOC, nontrivial topology, and superconductivity, together with the versatile tunability by surface functionalization or varying the substrate, collectively make few-layer stanene a fertile ground for studying novel superconductivity and tunable topological properties for potential applications in quantum devices, all based on a single-element system.

We thank the Ministry of Science and Technology of China (Grants No. 2019YFA0308600, No. 2020YFA0309000, and No. 2017YFA0303500),

NSFC (Grants No. 11521404, No. 11634009, No. 12174252, No. 92065201, No. 11874256, No. 11874258, No. 12074247, No. 11790313, No. 11861161003, No. 11634011, No. 11974323, and No. 11722435), the Strategic Priority Research Program of Chinese Academy of Sciences (Grants No. XDB28000000 and No. XDB30000000), the Science and Technology Commission of Shanghai Municipality (Grants No. 2019SHZDZX01, No. 19JC1412701, and No. 20QA1405100), and the Anhui Initiative in Quantum Information Technologies (Grant No. AHY170000) for partial support. C. Zhao gratefully acknowledges support from the PHD Graduate Development Scholarship of Shanghai Jiao Tong University.

* cuipeg@ustc.edu.cn

† jfjia@sytu.edu.cn

- [1] L. Fu and C. L. Kane, *Phys. Rev. Lett.* **100**, 096407 (2008).
- [2] X.-L. Qi and S.-C. Zhang, *Rev. Mod. Phys.* **83**, 1057 (2011).
- [3] M. Z. Hasan and C. L. Kane, *Rev. Mod. Phys.* **82**, 3045 (2010).
- [4] C. Beenakker, *Annu. Rev. Condens. Matter Phys.* **4**, 113 (2013).
- [5] M.-X. Wang, C. Liu, J.-P. Xu, F. Yang, L. Miao, M.-Y. Yao, C. Gao, C. Shen, X. Ma, X. Chen *et al.*, *Science* **336**, 52 (2012).

- [6] V. Mourik, K. Zuo, S. M. Frolov, S. Plissard, E. E. Bakkers, and L. P. Kouwenhoven, *Science* **336**, 1003 (2012).
- [7] S. Nadjperge, I. K. Drozdov, J. Li, H. Chen, S. Jeon, J. Seo, A. H. Macdonald, B. A. Bernevig, and A. Yazdani, *Science* **346**, 602 (2014).
- [8] J. P. Xu, M. X. Wang, Z. L. Liu, J. F. Ge, X. Yang, C. Liu, Z. A. Xu, D. Guan, C. L. Gao, D. Qian *et al.*, *Phys. Rev. Lett.* **114**, 017001 (2015).
- [9] H.-H. Sun, K.-W. Zhang, L.-H. Hu, C. Li, G.-Y. Wang, H.-Y. Ma, Z.-A. Xu, C.-L. Gao, D.-D. Guan, Y.-Y. Li *et al.*, *Phys. Rev. Lett.* **116**, 257003 (2016).
- [10] B. Jäck, Y. Xie, J. Li, S. Jeon, B. A. Bernevig, and A. Yazdani, *Science* **364**, 1255 (2019).
- [11] J.-X. Yin, Z. Wu, J. Wang, Z. Ye, J. Gong, X. Hou, L. Shan, A. Li, X. Liang, X. Wu *et al.*, *Nat. Phys.* **11**, 543 (2015).
- [12] D. Wang, L. Kong, P. Fan, H. Chen, S. Zhu, W. Liu, L. Cao, Y. Sun, S. Du, J. Schneeloch *et al.*, *Science* **362**, 333 (2018).
- [13] Z. Wang, J. O. Rodriguez, L. Jiao, S. Howard, M. Graham, G. Gu, T. L. Hughes, D. K. Morr, and V. Madhavan, *Science* **367**, 104 (2020).
- [14] P. Zhang, Z. Wang, X. Wu, K. Yaji, Y. Ishida, Y. Kohama, G. Dai, Y. Sun, C. Bareille, K. Kuroda *et al.*, *Nat. Phys.* **15**, 41 (2019).
- [15] Q. Liu, C. Chen, T. Zhang, R. Peng, Y.-J. Yan, C.-H.-P. Wen, X. Lou, Y.-L. Huang, J.-P. Tian, X.-L. Dong, G.-W. Wang, W.-C. Bao, Q.-H. Wang, Z.-P. Yin, Z.-X. Zhao, and D.-L. Feng, *Phys. Rev. X* **8**, 041056 (2018).
- [16] M. Liao, Y. Zang, Z. Guan, H. Li, Y. Gong, K. Zhu, X. Hu, D. Zhang, Y. Xu, Y. Wang *et al.*, *Nat. Phys.* **14**, 344 (2018).
- [17] J. Falson, Y. Xu, M. Liao, Y. Zang, K. Zhu, C. Wang, Z. Zhang, H. Liu, W. Duan, K. He *et al.*, *Science* **367**, 1454 (2020).
- [18] Y. Xu, B. Yan, H.-J. Zhang, J. Wang, G. Xu, P. Tang, W. Duan, and S.-C. Zhang, *Phys. Rev. Lett.* **111**, 136804 (2013).
- [19] B.-H. Chou, Z.-Q. Huang, C.-H. Hsu, F.-C. Chuang, Y.-T. Liu, H. Lin, and A. Bansil, *New J. Phys.* **16**, 115008 (2014).
- [20] Y. Xu, P. Tang, and S.-C. Zhang, *Phys. Rev. B* **92**, 081112 (R) (2015).
- [21] D. Wang, L. Chen, X. Wang, G. Cui, and P. Zhang, *Phys. Chem. Chem. Phys.* **17**, 26979 (2015).
- [22] F. Yun, D. L. Cortie, and X. Wang, *Phys. Chem. Chem. Phys.* **19**, 25574 (2017).
- [23] Y. Liu, N. Gao, J. Zhuang, C. Liu, J. Wang, W. Hao, S. X. Dou, J. Zhao, and Y. Du, *J. Phys. Chem. Lett.* **10**, 1558 (2019).
- [24] F. Zhu, W. Chen, Y. Xu, C. Gao, D. Guan, C. Liu, D. Qian, S. Zhang, and J. Jia, *Nat. Mater.* **14**, 1020 (2015).
- [25] J. Gou, L. Kong, H. Li, Q. Zhong, W. Li, P. Cheng, L. Chen, and K. Wu, *Phys. Rev. Mater.* **1**, 054004 (2017).
- [26] C. Z. Xu, Y. H. Chan, P. Chen, X. Wang, D. Flototto, J. A. Hlevyack, G. Bian, S. K. Mo, M. Y. Chou, and T. C. Chiang, *Phys. Rev. B* **97**, 035122 (2018).
- [27] Y. Zang, T. Jiang, Y. Gong, Z. Guan, C. Liu, M. Liao, K. Zhu, Z. Li, L. Wang, W. Li *et al.*, *Adv. Funct. Mater.* **28**, 1802723 (2018).
- [28] J. Deng, B. Xia, X. Ma, H. Chen, H. Shan, X. Zhai, B. Li, A. Zhao, Y. Xu, W. Duan *et al.*, *Nat. Mater.* **17**, 1081 (2018).
- [29] X. Zheng, J.-F. Zhang, B. Tong, and R.-R. Du, *2D Mater.* **7**, 011001 (2020).
- [30] L. Zhang, W. Qin, L. Li, S. Li, P. Cui, Y. Jia, and Z. Zhang, *Nanoscale* **10**, 18988 (2018).
- [31] M. Copel, M. C. Reuter, E. Kaxiras, and R. M. Tromp, *Phys. Rev. Lett.* **63**, 632 (1989).
- [32] Z. Zhang and M. G. Lagally, *Science* **276**, 377 (1997).
- [33] See Supplemental Material at <http://link.aps.org/supplemental/10.1103/PhysRevLett.128.206802> for the calculational and experimental details, which includes Refs. [34–54].
- [34] P. Redhead, *AIP Conf. Proc.* **671**, 243 (2003).
- [35] C. G. Van de Walle, *Phys. Rev. Lett.* **85**, 1012 (2000).
- [36] M. K. Gupta, A. Priyadarshi, and Z. Khan, *Mater. Today Proc.* **2**, 1074 (2015).
- [37] G. Kresse and J. Furthmüller, *Phys. Rev. B* **54**, 11169 (1996).
- [38] P. E. Blöchl, *Phys. Rev. B* **50**, 17953 (1994).
- [39] G. Kresse and D. Joubert, *Phys. Rev. B* **59**, 1758 (1999).
- [40] J. P. Perdew, K. Burke, and M. Ernzerhof, *Phys. Rev. Lett.* **77**, 3865 (1996).
- [41] S. Grimme, J. Antony, S. Ehrlich, and H. Krieg, *J. Chem. Phys.* **132**, 154104 (2010).
- [42] P. Hofmann, *Prog. Surf. Sci.* **81**, 191 (2006).
- [43] A. A. Soluyanov and D. Vanderbilt, *Phys. Rev. B* **83**, 235401 (2011).
- [44] M. L. Sancho, J. L. Sancho, J. L. Sancho, and J. Rubio, *J. Phys. F* **15**, 851 (1985).
- [45] A. A. Mostofi, J. R. Yates, Y.-S. Lee, I. Souza, D. Vanderbilt, and N. Marzari, *Comput. Phys. Commun.* **178**, 685 (2008).
- [46] Q. Wu, S. Zhang, H.-F. Song, M. Troyer, and A. A. Soluyanov, *Comput. Phys. Commun.* **224**, 405 (2018).
- [47] Y. Jia, B. Wu, H. H. Weitering, and Z. Zhang, *Phys. Rev. B* **74**, 035433 (2006).
- [48] L. Li, J. Zeng, W. Qin, P. Cui, and Z. Zhang, *Nano Energy* **58**, 40 (2019).
- [49] X. Qian, J. Liu, L. Fu, and J. Li, *Science* **346**, 1344 (2014).
- [50] T. Li, P. Wang, H. Fu, L. Du, K. A. Schreiber, X. Mu, X. Liu, G. Sullivan, G. A. Csáthy, X. Lin, and R.-R. Du, *Phys. Rev. Lett.* **115**, 136804 (2015).
- [51] S. Takatani and Y.-W. Chung, *Phys. Rev. B* **31**, 2290 (1985).
- [52] Y. Zhang, C. H. Wong, J. Shen, S. T. Sze, B. Zhang, H. Zhang, Y. Dong, H. Xu, Z. Yan, Y. Li *et al.*, *Sci. Rep.* **6**, 1 (2016).
- [53] P. A. Frigeri, D. F. Agterberg, A. Koga, and M. Sigrist, *Phys. Rev. Lett.* **92**, 097001 (2004).
- [54] J.-P. Xu, C. Liu, M.-X. Wang, J. Ge, Z.-L. Liu, X. Yang, Y. Chen, Y. Liu, Z.-A. Xu, C.-L. Gao, D. Qian, F.-C. Zhang, and J.-F. Jia, *Phys. Rev. Lett.* **112**, 217001 (2014).
- [55] B. A. Bernevig, T. L. Hughes, and S.-C. Zhang, *Science* **314**, 1757 (2006).
- [56] I. K. Drozdov, A. Alexandradinata, S. Jeon, S. Nadj-Perge, H. Ji, R. Cava, B. A. Bernevig, and A. Yazdani, *Nat. Phys.* **10**, 664 (2014).
- [57] S. Tang, C. Zhang, D. Wong, Z. Pedramrazi, H.-Z. Tsai, C. Jia, B. Moritz, M. Claassen, H. Ryu, S. Kahn *et al.*, *Nat. Phys.* **13**, 683 (2017).
- [58] J. L. Collins, A. Tadich, W. Wu, L. C. Gomes, J. N. Rodrigues, C. Liu, J. Hellerstedt, H. Ryu, S. Tang, S.-K. Mo *et al.*, *Nature (London)* **564**, 390 (2018).
- [59] F. Schindler, Z. Wang, M. G. Vergniory, A. M. Cook, A. Murani, S. Sengupta, A. Y. Kasumov, R. Deblock, S. Jeon, I. Drozdov *et al.*, *Nat. Phys.* **14**, 918 (2018).

- [60] C. Zhao, M. Hu, J. Qin, B. Xia, C. Liu, S. Wang, D. D. Guan, Y. Li, H. Zheng, J. Liu, and J. Jia, *Phys. Rev. Lett.* **125**, 046801 (2020).
- [61] S. Murakami, *Phys. Rev. Lett.* **97**, 236805 (2006).
- [62] Z. Liu, C.-X. Liu, Y.-S. Wu, W.-H. Duan, F. Liu, and J. Wu, *Phys. Rev. Lett.* **107**, 136805 (2011).
- [63] G. Wu, H. Chen, Y. Sun, X. Li, P. Cui, C. Franchini, J. Wang, X.-Q. Chen, and Z. Zhang, *Sci. Rep.* **3**, 1233 (2013).
- [64] S. Hart, H. Ren, T. Wagner, P. Leubner, M. Mühlbauer, C. Brüne, H. Buhmann, L. W. Molenkamp, and A. Yacoby, *Nat. Phys.* **10**, 638 (2014).
- [65] H.-H. Sun, M.-X. Wang, F. Zhu, G.-Y. Wang, H.-Y. Ma, Z.-A. Xu, Q. Liao, Y. Lu, C.-L. Gao, Y.-Y. Li *et al.*, *Nano Lett.* **17**, 3035 (2017).
- [66] F. Lpke, D. Waters, S. C. d. l. Barrera, D. G. Widom, Michael Mandrus, J. Yan, R. M. Feenstra, and B. M. Hunt, *Nat. Phys.* **16**, 526 (2020).
- [67] E. Sajadi, T. Palomaki, Z. Fei, W. Zhao, P. Bement, C. Olsen, S. Luescher, X. Xu, J. A. Folk, and D. H. Cobden, *Science* **362**, 922 (2018).
- [68] V. Fatemi, S. Wu, Y. Cao, L. Bretheau, Q. D. Gibson, K. Watanabe, T. Taniguchi, R. J. Cava, and P. Jarillo-Herrero, *Science* **362**, 926 (2018).